

Stick-slip instabilities and shear strain localization in amorphous materialsEric G. Daub^{1,2,*} and Jean M. Carlson²¹*Geophysics Group and Center for Nonlinear Studies, Los Alamos National Laboratory, Los Alamos, New Mexico, 87545 USA*²*Department of Physics, University of California, Santa Barbara, California, 93106 USA*

(Received 8 September 2009; published 15 December 2009)

We study the impact of strain localization on the stability of frictional slipping in dense amorphous materials. We model the material using shear transformation zone (STZ) theory, a continuum approximation for plastic deformation in amorphous solids. In the STZ model, the internal state is quantified by an effective disorder temperature, and the effective temperature dynamics capture the spontaneous localization of strain. We study the effect of strain localization on stick-slip instabilities by coupling the STZ model to a noninertial spring slider system. We perform a linear stability analysis to generate a phase diagram that connects the small scale physics of strain localization to the macroscopic stability of sliding. Our calculations determine the values of spring stiffness and driving velocity where steady sliding becomes unstable and we confirm our results through numerical integration. We investigate both homogeneous deformation, where no shear band forms, and localized deformation, where a narrow shear band spontaneously forms and accommodates all of the deformation. Our results show that at a given velocity, strain localization leads to unstable frictional sliding at a much larger spring stiffness compared to homogeneous deformation, and that localized deformation cannot be approximated by a homogeneous model with a narrower material. We also find that strain localization provides a physical mechanism for irregular stick-slip cycles in certain parameter ranges. Our results quantitatively connect the internal physics of deformation in amorphous materials to the larger scale frictional dynamics of stick-slip.

DOI: [10.1103/PhysRevE.80.066113](https://doi.org/10.1103/PhysRevE.80.066113)

PACS number(s): 62.20.F-, 83.10.Gr, 71.55.Jv, 46.35.+z

I. INTRODUCTION

Dense amorphous materials include a wide range of systems, including granular materials, glassy materials, colloids, emulsions, and possibly even biological tissue. These materials often serve as lubricants for sheared interfaces, ranging in scale from atomically thin films to earthquake faults. While they differ vastly in scale, each is made up of a collection of smaller particles—the thin film contains a few layers of molecules, while the earthquake fault is filled with crushed grains of rock. Both the interfacial material and the large scale system as a whole can exhibit rich and complex dynamics. Most studies of these systems focus on the small scale physics in the material or the large scale dynamics of friction. In this paper, we bridge the two approaches using a constitutive law derived from small scale physics to investigate instabilities in both the deformation in the interfacial layer and the macroscopic friction.

Laboratory experiments show that granular materials [1], fault rocks [2–4], and thin films [5–8] exhibit similar frictional dynamics, including a yield stress, hysteresis, rate dependent frictional resistance, and stick-slip. In this study, we focus on stick-slip instabilities, which are responsible for earthquake slip on seismic faults, noise from automobile brakes and tires, music from a violin, and excessive wear on frictional interfaces in machinery. Modeling the dynamics of friction in these materials is a challenging problem, as models must resolve the microscopic physics of deformation and simultaneously remain tractable for capturing the large scale behavior.

Experimental observations of friction are sometimes directly incorporated into phenomenological friction laws, such as the Stribeck curve [9] and the Dieterich-Ruina rate and state dependent friction laws [10,11]. These fits to data capture many important features of experiments, but to date have not been derived from microscopic physics and do not resolve internal dynamic instabilities within the interfacial layer. Molecular dynamics simulations have provided extensive information about microscopic deformation and flow, but only for limited numbers of particles and a narrow range of time scales. Stick-slip motion has been explored in the context of constitutive models [12–15] and molecular dynamics simulations [16,17].

In this paper, we use a physics-based constitutive model that combines insights from atomistic simulations with the tractability of a constitutive law to connect macroscopic friction dynamics to the small scale physics of deformation. Our friction model is based on the theory of shear transformation zones (STZs) [18,19]. This continuum approach incorporates features from molecular dynamics simulations and fundamental constraints from nonequilibrium statistical physics and has been applied to a wide variety of materials [15,20,21]. The STZ constitutive model provides physical insight into plastic deformation, but is tractable for studying larger scale sheared interfaces. Additionally, STZ theory has sufficient resolution of the microscopic scale to capture shear band instabilities and the spontaneous localization of strain [22–24]. When a shear band forms, deformation localizes to a region that is much narrower than the thickness of the material. Localization plays an important role in the frictional properties of bulk metallic glasses [25], granular materials [26], and bubble rafts [27].

In this study, we determine the effect of the microscopic physics of strain localization on the dynamics of stick-slip.

*edaub@lanl.gov

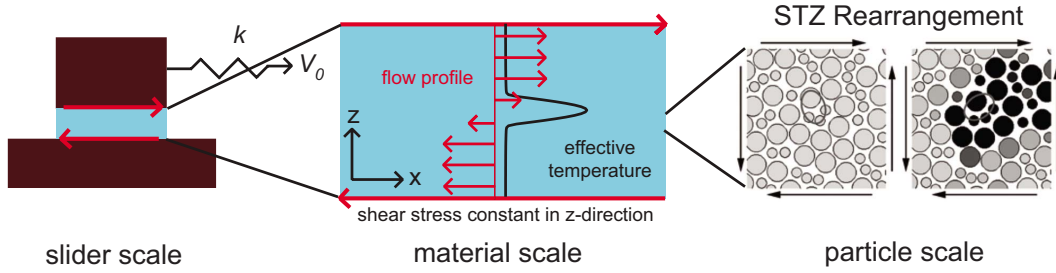


FIG. 1. (Color online) Illustration of the spring slider modeled with STZ theory. (Left) A block of negligible mass is pulled by a spring of stiffness k at constant velocity V_0 . An amorphous material lubricates the sheared interface. (Center) A close up of the amorphous material indicates that we resolve the dynamic evolution of strain inside the material. In STZ theory, the microscopic physics is captured through the evolution of an effective temperature, which is heterogeneous within the material. Our model accounts for the effect of strain localization on the motion of the block. (Right) Close up of an STZ reversal at the particle scale. As the material is sheared, an ellipse has drawn through the particles switches from one orientation to the other. The dark particles on the right indicate where plastic deformation has occurred in the material. STZ image taken from Falk and Langer [18].

We perform a linear stability analysis with the STZ equations to quantitatively determine how small scale localization impacts the large scale frictional behavior. We compare localized strain, where a shear band dynamically forms, to homogeneous deformation, where no shear band forms and the strain rate is spatially uniform across the interfacial layer. We find that localization alters the parameter range where stick-slip occurs, thus demonstrating that the small scale physics plays an important role in the large scale dynamics of friction.

We begin with a discussion of the physics behind the STZ model and the block slider equations in Section II. In Sec. III, we present the results of our stability analysis and our numerical studies with the STZ model. Section IV concludes with a discussion of the implications of our work for friction and deformation in amorphous materials.

II. MODEL EQUATIONS

A. STZ constitutive law

We model the constitutive response of the interfacial material with STZ theory. STZ theory is a continuum approximation for amorphous solids under shear. It was originally developed to model deformation and fracture in a Lennard-Jones glass [18,19], but has also been applied to boundary lubrication [15], granular flow [28], and dynamic earthquake rupture [21]. Recently it has been shown that STZ theory captures the dynamic instability that leads to the formation of shear bands in glassy materials [22,24] and in dynamic earthquake rupture [23]. In this section, we discuss the physics behind the STZ model and present the basic equations. A detailed derivation of the STZ equations is presented in Appendix A for completeness.

We consider a spring slider with negligible mass (i.e., overdamped). The spring is pulled at a constant velocity V_0 . The slider is illustrated on the left in Fig. 1. The sheared interface is filled with an amorphous material. The material has a finite thickness of $2w$ in the z direction, and is much larger and translationally invariant in the other spatial directions, reducing the spatial dependence to z only. We also assume that the material is symmetric about $z=0$, and there-

fore we only model the material for $0 \leq z \leq w$. A close up of the amorphous material (center in Fig. 1) shows that the shear strain can be heterogeneous within the material layer.

In STZ theory, when a collection of particles is sheared, the resulting particle displacements can be written as the sum of two components: affine displacements, where the particle motion is uniform throughout the material, and nonaffine displacements, where the particle motion is heterogeneous. Affine displacements result in an elastic material response, while nonaffine displacements can produce plastic deformation. Nonaffine deformation can contribute to the elastic response, but STZ theory makes the simplifying assumption that the nonaffine deformation is purely plastic.

In simulations and experiments with dense amorphous materials, nonaffine deformation tends to occur in localized regions as particles rearrange from one metastable orientation to another [18,19]. These zones are referred to as STZs. An STZ switching between the two orientations is shown at the right in Fig. 1. STZ theory assumes that all nonaffine deformation occurs in these zones. Each switch accumulates a fixed strain increment and a minimum shear stress must be applied for the switch to occur. Once an STZ has switched in the direction of applied shear, it cannot accumulate further plastic strain in that direction. Therefore, to allow the material to accumulate further plastic strain, STZs are created and destroyed as the material is sheared and energy is dissipated. Once STZs flip in the direction of applied shear, they are destroyed, and STZs must be created in the opposite orientation to maintain steady plastic deformation.

The plastic strain rate $\dot{\gamma}$ depends on two factors: the number of STZs, and the rate at which STZs switch between orientations. The shear stress τ determines the rate at which STZs change orientation, and the total number of STZs is governed by an effective disorder temperature χ [29]. These factors are summarized by the following equation:

$$\dot{\gamma} = \frac{1}{t_0} f(\tau) \exp(-1/\chi). \quad (1)$$

This equation shows that the plastic strain rate depends on the shear stress through the function $f(\tau)$, and the effective temperature through the Boltzmann factor $\exp(-1/\chi)$. Also

included in Eq. (1) is the characteristic time for STZ reversals t_0 , an important time scale in the problem. We adopt an exponential form for $f(\tau)$, which is discussed in the full derivation of the STZ equations in Appendix A.

The effective disorder temperature evolves dynamically as the material is driven away from equilibrium. The governing partial differential equation that we adopt for the effective temperature is

$$\dot{\chi} = \frac{\dot{\gamma}\tau}{c_0\tau_y} \left(1 - \frac{\chi}{\hat{\chi}(\dot{\gamma})} \right) + \frac{\partial}{\partial z} \left(D\dot{\gamma} \frac{\partial \chi}{\partial z} \right). \quad (2)$$

The effective temperature evolution equation includes terms for energy dissipation and diffusion. The dissipation term indicates that as plastic work is done on the system, the particles are stirred. This drives the effective temperature toward its steady-state value $\hat{\chi}(\dot{\gamma})$, which is a function of the plastic strain rate. Diffusion of effective temperature is observed in simulations [30], and occurs with a time scale given by the inverse strain rate and a length scale \sqrt{D} . The diffusion length is determined by the particles in the amorphous material—this length might scale with a characteristic particle diameter in a granular material, or a typical interparticle separation in a glass. Note that because the time scale for diffusion is the inverse plastic strain rate, diffusion of effective temperature occurs only when the material is sheared.

The steady-state effective temperature $\hat{\chi}(\dot{\gamma})$ is given by [20]

$$\hat{\chi}(\dot{\gamma}) = \frac{\chi_w}{\log\left(\frac{q_0}{t_0\dot{\gamma}}\right)}. \quad (3)$$

This form for $\hat{\chi}(\dot{\gamma})$ is based on simulations of a glass by Haxton and Liu [31]. Parameters include the effective temperature activation barrier χ_w and the nondimensional strain rate where STZ theory breaks down q_0 . For strain rates larger than $\dot{\gamma} = q_0/t_0$, the effective temperature diverges and plastic deformation no longer occurs as localized STZs. The effective temperature activation barrier χ_w is a very important parameter, as it determines the frictional rate dependence. If $\chi_w > 1$, then the material is rate strengthening, which means that the steady-state shear stress increases with the strain rate. If $\chi_w < 1$, then the material is rate weakening, and as the strain rate increases, the steady-state shear stress decreases.

We also need boundary conditions on the effective temperature at the material edges. We assume that there is no effective temperature flux out of the boundaries of the amorphous material, so $\partial\chi/\partial z = 0$ at $z = \pm w$.

The STZ equations capture the spontaneous localization of strain in amorphous materials. Localization occurs because of an instability in the effective temperature dynamics. If the effective temperature is *a priori* spatially homogeneous, then by symmetry all subsequent deformation is homogeneous. The diffusion term in Eq. (2) is zero and the effective temperature evolves in time but does not vary in space. This produces homogeneous deformation, i.e., the strain rate is uniform across the amorphous material (z direction). If the effective temperature is homogeneous, the STZ

equations produce a logarithmic frictional rate dependence that matches the rate dependence of the laboratory derived Dieterich-Ruina friction laws that are frequently used in seismology [21].

However, a perfectly uniform effective temperature is not physically realistic. If there is any heterogeneity in the effective temperature, then some spatial regions have more STZs, and therefore a larger strain rate. The energy dissipation term in Eq. (2) is proportional to the strain rate and the effective temperature grows more quickly in regions where the effective temperature is larger. This instability amplifies small inhomogeneities and the end result of heterogeneous initial conditions is deformation in a single narrow shear band.

Although truly homogeneous deformation is not a physically realistic scenario, in many cases it is a reasonable approximation and therefore provides a natural comparison with deformation in a localized shear band. If the material is very thin, the shear band that forms may be wider than the material. For example, boundary lubrication experiments are often done with thin films that are only a few molecules thick. In this case, homogeneous deformation serves as a good approximation because the effective temperature varies over a length scale that is larger than the material thickness. We analyze both the homogeneous approximation and the full STZ equations with localization in our study to determine the role of the physics of strain localization on frictional sliding.

B. Block slider equations

To explore the implications of microscopic strain localization on macroscopic friction, we couple the STZ equations [Eqs. (1) and (2)] to a spring slider. A block is attached to a spring pulled at a constant rate, and the block motion causes shear deformation in the amorphous material (left in Fig. 1). For simplicity we ignore inertial effects. Experimental data often exhibits stick-slip motion in overdamped regimes [32], where the block oscillation time is much smaller than the duration of a stick-slip event. In this regime the frictional time scales are more important for the block dynamics than inertial effects. Because we are in an overdamped regime, the friction force balances the spring force. Therefore, we only require a dynamic equation for the frictional shear stress τ in the amorphous material to complete the system of equations describing the STZ block slider model. Here τ is taken to be constant in the z direction. This follows from our assumption that the stress equilibration time scale is much faster than the time scales in the STZ friction law; the static solution to the momentum conservation equations in this geometry is a spatially uniform shear stress.

Stress in the material evolves due to elastic and plastic deformation. The spring of stiffness k is pulled at a constant rate V_0 , which increases the shear stress by extending the spring. Meanwhile, plastic deformation occurs in the amorphous solid and causes the material to soften. Therefore, the shear stress τ evolves according to

$$\dot{\tau} = k \left(V_0 - \int_0^w \dot{\gamma} dz \right). \quad (4)$$

Here, dots represent a time derivative. The first term on the right-hand side represents elastic loading from the spring and

the second term represents material softening at a rate determined by the spatial integral of the plastic strain rate $\dot{\gamma}$. Because the system is overdamped, the spatial integral of the plastic strain rate over the entire material width is also the velocity of the slider block. The plastic strain rate is given by the STZ equation [Eq. (1)] and is a function of the stress and the effective temperature.

C. Time scales

The block slider equation [Eq. (4)], along with the STZ equations [Eqs. (1) and (2)], involve a number of different time scales. The fastest among these is the STZ rearrangement time t_0 . An estimate for t_0 is a molecular vibrational time scale for a glassy material or a characteristic particle diameter divided by the speed of sound in a granular material. These time scales are much faster than all others in the problem, and rearrangements are taken to be instantaneous in the STZ model.

The time scale for stress equilibration in the material is of the order of the thickness of the layer divided by the speed of sound. Note that since the layer contains many particles, this is certainly much slower than an individual STZ rearrangement. This time scale is also taken to be instantaneous in the model, which is implicit in Eq. (4). For the theory to be applicable, all other processes must be slower than stress equilibration.

The time scale for effective temperature evolution is the inverse plastic strain rate. This describes both energy dissipation and diffusion and it must be slower than the stress equilibration time. Large strain rates tend to occur for large driving rates V_0 , and also for stick-slip motion when the spring is very compliant. This restricts the range of driving rates as we numerically integrate the equations.

Because we assume that the slider is overdamped, we ignore the inertia of the block. This amounts to taking the time scale for oscillations of the spring slider to be much faster than the inverse plastic strain rate. The duration of a stick-slip event is thus much longer than the natural oscillation period of the unencumbered block and spring, which means that the frictional time scale dictates the dynamics of stick slip. Stick slip can also occur in an underdamped regime with a larger block mass, but we do not consider that limit in our analysis.

D. Nondimensional equations

We nondimensionalize the equations using the following parameters: scale all times by the STZ rearrangement time t_0 , scale all lengths by the material width w , and scale all stresses by the STZ yield stress τ_y . The parameters can thus be redefined as follows: stress $\tau' = \tau / \tau_y$, strain rate $\dot{\gamma}' = t_0 \dot{\gamma}$, driving rate $V'_0 = V_0 t_0 / w$, STZ activation stress $\sigma'_d = \sigma_d / \tau_y$, diffusion length scale $D' = D / w^2$, and spring constant $k' = kw / \tau_y$. The nondimensional equations are (dropping all primes on variables)

$$\dot{\tau} = k \left(V_0 - \int_0^1 \dot{\gamma} dz \right), \quad (5)$$

TABLE I. Dimensionless parameters for the block slider equations.

Parameter	Description
$\epsilon=10$	Strain accumulated per STZ reversal
$\sigma_d=1$	STZ activation stress
$f_0=11.5$	STZ activation energy
$c_0=1$	Effective temperature specific heat
$D=0.1$	Squared effective temperature diffusion length scale
$\chi_w=0.8$	Effective temperature activation energy
$q_0=1$	Strain rate at which STZ theory breaks down
$V_0=\text{varies}$	Driving rate
$k=\text{varies}$	spring constant

$$\dot{\chi} = \frac{\dot{\gamma}\tau}{c_0} \left(1 - \frac{\chi}{\hat{\chi}(\dot{\gamma})} \right) + \frac{\partial}{\partial z} \left(D \dot{\gamma} \frac{\partial \chi}{\partial z} \right). \quad (6)$$

where $\hat{\chi}(\dot{\gamma}) = \chi_w / \log(q_0 / \dot{\gamma})$ and $\dot{\gamma} = f(\tau) \exp(-1/\chi)$. The stress factor is given by $f(\tau) = 2\epsilon \exp(-f_0) \cosh(\tau / \sigma_d) (1 - 1/\tau)$.

The nondimensional parameters that we use in numerical integration of the block slider model are given in Table I. We keep all parameters constant except the driving rate and spring stiffness, which we vary to explore the parameter ranges that lead to stick-slip motion.

E. Small scale effects on friction in STZ theory

In STZ theory, the dynamics of friction is controlled by the evolution of the effective temperature. The effective temperature is derived from the underlying statistical physics of dense, disordered solids and STZ theory connects macroscopic frictional behavior to the evolution of the effective temperature. This includes resolving the spontaneous localization of strain. Other friction laws that do not resolve the internal dynamics of the interfacial material are *a priori* incapable of resolving the dynamical shear band instability.

Manning *et al.* [24] showed that a key parameter that connects the microscopic physics to the macroscopic dynamics in STZ theory is the effective temperature activation barrier χ_w . Manning *et al.* performed a linear stability analysis of the STZ equations and showed that χ_w determined the stability of deformation with a spatially uniform effective temperature. If this activation barrier is less than unity, homogeneous deformation is linearly unstable ($\chi_w < 1$). This is precisely the condition for rate weakening friction. Rate weakening refers to the strain rate dependence of the steady-state shear stress—as the strain rate increases, the steady-state stress decreases. Therefore, rate weakening materials always form shear bands given any heterogeneity in the initial effective temperature, as steady sliding is linearly unstable. If the activation barrier is less than unity, then steady sliding is stable. This corresponds to the parameter range for rate strengthening friction, where the shear stress increases as the strain rate increases. However, shear bands can still form if $\chi_w > 1$ due to transient effects [22,24].

Although shear bands form for both rate weakening and rate strengthening materials, we focus on rate weakening materials in this study. Previous studies with Dieterich-Ruina friction [12] and STZ theory without strain localization [15] showed that rate weakening is required for steady sliding to be unstable in a single degree of freedom elastic system. When shear band formation is included, we also find that steady sliding is unstable only if friction is rate weakening, which we show in the next section.

III. STICK-SLIP DYNAMICS

In this section, we explore the dynamics of the block slider model with STZ theory. We investigate the effects of shear band formation on the stability of frictional sliding and generate a phase diagram that distinguishes between parameters that produce stick-slip versus steady sliding with and without shear bands. We also identify more exotic stick-slip cycles and connect the underlying microscopic physics to the observed complex dynamics. This involves both analytical and numerical studies with the STZ equations.

For fixed material parameters, the type of motion depends on the driving rate (the speed at which the spring is loaded) and the stiffness of the spring. If we fix the spring stiffness, large driving velocities result in steady sliding of the block. The slider moves at the same velocity as the load point (the end of the spring that is pulled at a constant velocity) and the shear stress is at its steady-state value. At slower driving rates, the block undergoes repeated stick-slip cycles. If we instead fix the driving velocity, stiff springs produce steady sliding and compliant springs produce stick-slip. The spring stiffness and the driving rate are both important for determining the slider dynamics, as observed in experiments [33].

In laboratory experiments, the transition from steady sliding to stick-slip is usually investigated by fixing the spring stiffness and varying the driving velocity, as it is much easier to change the driving velocity in an experiment. In STZ theory, it is more straightforward to calculate the stiffness at which sliding becomes unstable as a function of velocity, because the velocity as a function of stiffness cannot be obtained in closed form. This is due to the nonlinear dependence of the stress and effective temperature on the driving rate. Ultimately, both approaches are equivalent as each determines the boundary in (V_0, k) space separating stick-slip and steady sliding. Because we solve for the stiffness as a function of velocity, we refer to the spring stiffness where the motion transitions from stable sliding to stick-slip as the critical stiffness $k_{crit}(V_0)$. Our analytical results focus on determining the critical stiffness as a function of the STZ parameters, allowing us to connect stick-slip to the microscopic physics of deformation.

An example of stick-slip with the STZ law is illustrated in Fig. 2, which shows shear stress as a function of the slider velocity for one cycle of the motion. The slider velocity is plotted on a logarithmic scale. The vertical line indicates the velocity at which the spring is pulled V_0 . At the left, the velocity is much smaller than the driving velocity V_0 and the slider “sticks” (i.e., creeps at a small velocity). As the spring is loaded, the shear stress increases until the spring over-

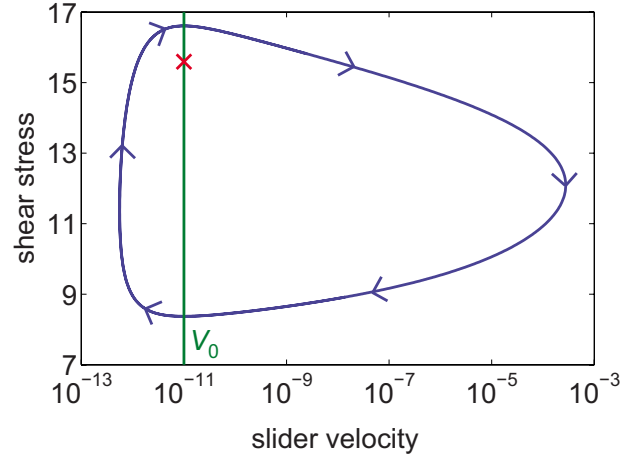


FIG. 2. (Color online) Stress and slider velocity evolution during periodic stick-slip motion with the STZ law. Instead of sliding steadily, which would be a single point on this diagram, the block cycles through successive stick and slip cycles. The x on the diagram indicates the steady sliding solution. At the far left, the block is moving much slower than the rate at which the spring is pulled (the vertical line), and the shear stress increases as the spring is extended. At the top, the spring force is large enough to initiate slip and the block slips rapidly relative to V_0 . The block overshoots the load point and the spring stops the block at the bottom of the loop. The cycle repeats as the stress build up again during the stick phase. Note that the slider velocity is not zero during a stick cycle—the block creeps much slower than the rate at which the spring is pulled, but never truly stops.

comes the frictional resistance. The block begins to slip much more rapidly than the rate at which the spring is pulled. The shear stress drops, and the block overshoots the load point, which causes it to stick again and the cycle repeats.

Stick-slip motion occurs when steady frictional sliding is unstable, as shown in Fig. 3. The plot shows the frictional stress as a function of the load point displacement. The slider begins sliding steadily, but the block motion transitions to repeated stick-slip cycles. The inset in Fig. 3(b) shows that stick-slip motion involves elastic loading by the spring over a large load point displacement during the stick phase. The stress drops very rapidly during the “slip” phase, indicating a large slider velocity.

A. Analytical results

Stick-slip instabilities occur when the steady sliding solution to the block slider equations becomes unstable to perturbations. The system of equations describing the block motion is

$$\begin{aligned} \dot{\tau} &= k(V_0 - f(\tau)) \int_0^1 \exp(-1/\chi) dz, \quad (7) \\ \dot{\chi} &= \frac{f(\tau) \exp(-1/\chi) \tau}{c_0} \left[1 - \frac{\chi}{\hat{\chi}(\dot{\gamma})} \right] + Df(\tau) \frac{\partial}{\partial z} \left[\exp(-1/\chi) \frac{\partial \chi}{\partial z} \right]. \quad (8) \end{aligned}$$

These are the same equations as Eqs. (5) and (6), with the strain rate written out explicitly in terms of the stress and

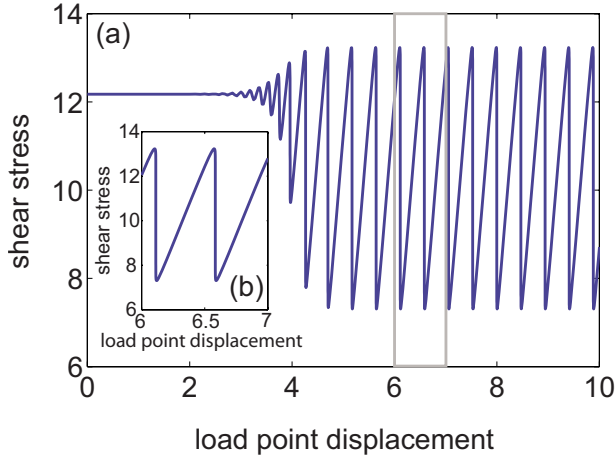


FIG. 3. (Color online) Shear stress as a function of load point displacement for stick-slip motion. The load point displacement refers to the displacement of the end of the spring that is pulled at a constant rate. (a) The block starts out sliding steadily, but steady sliding is unstable and the motion evolves into stick-slip cycles. (b) The inset shows a close up of stable, periodic stick-slip cycle, shown in Fig. 2, contained in the gray box of the main figure. The stress increases during the stick phase due to the elastic loading of the spring, while the rapid slip of the block suddenly drops the stress during the slip phase.

effective temperature. We analytically determine the critical stiffness using a linear stability analysis of the STZ equations. In Sec. III B, we confirm the results by numerically integrating the block slider model.

Linear stability analysis determines if perturbations to the stress and effective temperature grow or decay in time. Mathematically, this involves finding the real part of the eigenvalues of the Jacobian. Negative real parts imply perturbations to the stress and effective temperature decay exponentially in time and steady sliding is stable. Positive real parts imply steady sliding is unstable, and perturbations to the stress and effective temperature grow exponentially in time.

The analysis is straightforward, though the intermediate expressions in the calculation are fairly complicated. We calculate stability criteria for homogeneous deformation, where the strain rate is uniform throughout the material, and for localized deformation, where the strain rate is determined by the dynamic evolution of the effective temperature. The details of the stability analysis are presented in Appendix B.

If deformation is homogeneous throughout the interfacial material, steady sliding is unstable if the following criteria is met,

$$-\frac{kV_0 f'(\tau)}{f(\tau)} + \frac{V_0 \tau}{c_0 \hat{\chi}} \left(\frac{1}{\chi_w} - 1 \right) > 0. \quad (9)$$

This expression is derived in Appendix B. For localized deformation, we examine the stability of deformation with a steady shear band, which is an approximate steady sliding solution to the block slider equations. This replaces the homogeneous solution when internal degrees of freedom of the

interfacial material are resolved. In the localized case, the instability criteria is

$$-\frac{kV_0 f'(\tau)}{f(\tau)} + \frac{\dot{\gamma} \tau}{c_0 \hat{\chi}} \left(\frac{1}{\chi_w} - 1 \right) - 2D \frac{\dot{\gamma}}{\chi^3} \left(\frac{\partial \chi}{\partial z} \right)^2 > 0. \quad (10)$$

For the derivation of this result, see Appendix B.

For both homogeneous and localized deformation, the stability criteria [Eqs. (9) and (10)] depend on several different terms. In both expressions, the first term comes from the spring force, which is always less than zero and is therefore always stabilizing. This term is identical for the two cases. The second term in both expressions results from energy dissipation in the amorphous material. This term can be greater than zero, and thus can be destabilizing. Note that for homogeneous deformation, the dissipation term is proportional to the driving rate V_0 , while for localized deformation, it is proportional to the plastic strain rate $\dot{\gamma}$. The strain rate in a shear band is larger than the overall driving rate, so localization makes energy dissipation more destabilizing. For localized deformation, the third term comes from diffusion. This term is always negative, and thus stabilizes steady sliding. The increase in the energy dissipation term is the larger effect, implying that localization results in stick-slip motion over a larger range of parameters. The stability criteria connect the microscopic physics of the effective temperature (the energy dissipation and diffusion terms) to the macroscopic frictional behavior (the stress term).

The critical stiffness is the stiffness at which the terms exactly cancel. For the homogeneous case this is simply

$$k_{crit,h}(V_0) = \frac{f(\tau) \tau (V_0)}{f'(\tau) c_0 \hat{\chi}(V_0)} \left(\frac{1}{\chi_w} - 1 \right). \quad (11)$$

To determine the critical stiffness for localized deformation, we must quantitatively determine the effect of localization (i.e., determine the strain rate and effective temperature in the shear band). We cannot do this analytically, as the effective temperature governing equation is highly nonlinear. We instead estimate it by assuming that to a first approximation, the strain rate is constant inside a shear band of thickness a and negligible outside the shear band. This means that the strain rate in the shear band is V_0/a and the effective temperature inside the shear band is $\hat{\chi}(V_0/a)$. We also must estimate $\partial \chi / \partial z$ to quantify the effect of diffusion. Because the strain rate is negligible outside the shear band, $\hat{\chi}$ is not defined, so we instead use the value of the effective temperature with driving rate V_0 , $\hat{\chi}(V_0)$. Therefore, if we have an estimate of the shear band thickness a , we can easily calculate $\dot{\gamma} = V_0/a$, $\hat{\chi}(V_0/a)$, and $\partial \chi / \partial z = (\hat{\chi}(V_0/a) - \hat{\chi}(V_0))/a$, and use these values to estimate the critical stiffness.

We estimate the shear band thickness a by assuming that dissipation and diffusion roughly balance in the shear band. Equating these terms gives

$$\frac{\dot{\gamma} \tau}{c_0} \sim D \dot{\gamma} \frac{\chi}{a^2}. \quad (12)$$

The strain rate divides out, and solving for a yields

$$a \sim \sqrt{\frac{Dc_0\chi}{\tau}}. \quad (13)$$

This expression shows that a scales with the diffusion length \sqrt{D} , but also depends on the stress, the effective temperature, and the effective temperature specific heat. Therefore, given the driving rate, we determine the steady-state shear stress and effective temperature, and use these values to predict a .

Tests of Eq. (13) through numerical integration show that the scaling for each of the parameters is correct. However, direct use of Eq. (13) underestimates a . This is because the energy dissipation term is smaller than the estimate of $\dot{\gamma}\tau/c_0$, as χ is not completely negligible compared to $\hat{\chi}$. A better estimate can be obtained by numerically integrating the STZ equations once to determine a constant of proportionality. We use the half width of the shear band at half the maximum strain rate as our estimate of a . This criterion predicts that the shear band thickness is about 3.7 times larger than in Eq. (13) for the parameters in Table I. The value of the critical stiffness is not very sensitive to this proportionality factor. If the factor is changed to 3 or 4.5, the critical stiffness decreases by about 10% in both cases. Both cases result in a decreased critical stiffness because there are two competing localization effects, dissipation, and diffusion. Increasing the proportionality factor changes the dissipation effect more than the diffusion effect, and decreasing the proportionality factor changes the diffusion effect more than the dissipation effect.

Therefore, the shear band thickness for the parameters in our simulations is

$$a = 3.7 \sqrt{\frac{Dc_0\hat{\chi}(V_0)}{\tau}}, \quad (14)$$

and the critical stiffness for localized deformation is

$$k_{crit,l}(V_0) = \frac{f(\tau)\tau(V_0)}{af'(\tau)c_0\hat{\chi}(V_0/a)} \left(\frac{1}{\chi_w} - 1 \right) - \frac{2Df(\tau)[\hat{\chi}(V_0/a) - \hat{\chi}(V_0)]^2}{[a\hat{\chi}(V_0/a)]^3 f'(\tau)}. \quad (15)$$

Equations (11) and (15) determine the boundaries for homogeneous and localized deformation in (k, V_0) space separating stick-slip and steady sliding. Above k_{crit} , steady sliding is stable, and below k_{crit} , stick-slip occurs. The expression for localized deformation differs from the homogeneous expression due to the diffusion term and the larger dissipation term. These changes have competing effects—diffusion stabilizes steady sliding, while dissipation promotes unstable sliding. The increase in the energy dissipation term has a larger effect and the critical stiffness is larger for localized shear than for homogeneous deformation. In both cases, rate weakening is required for steady sliding to be unstable (if $\chi_w > 1$, then the critical stiffness would have to be negative, which is unphysical). The function $f(\tau)$ is determined by the stress dependence of the rate switching factor. In the case of exponential stress dependence, $f(\tau)/f'(\tau) \approx \sigma_d$, and the critical stiffness is proportional to the steady sliding stress and inversely proportional to the effective temperature. Note that

the stress and effective temperature are both functions of the driving velocity V_0 , which means that the critical stiffness depends on V_0 for both types of deformation. The stress decreases with increasing driving rate (since friction is rate weakening), and the effective temperature increases with the driving rate. This means that as the driving rate increases, the critical stiffness decreases, which is consistent with experiments [33]. This rate dependence is not captured by Dieterich-Ruina friction, which predicts that the critical stiffness is independent of the driving rate.

An important implication of our analysis is that localized deformation cannot be approximated by homogeneous deformation with a reduced material thickness. This is because the diffusion term in Eq. (15) reduces the critical stiffness, an effect that the homogeneous model cannot incorporate. It is necessary to resolve the internal material instabilities in order to produce the correct macroscopic behavior.

B. Numerical results

We confirm our analytic predictions for the dependence of the critical stiffness on the driving rate through numerical integration of the STZ equations. We perform numerical simulations to ensure that our estimate for the shear band thickness is accurate and to explore the connection between the internal disorder characterized by the effective temperature and irregular stick-slip dynamics.

We integrate Eqs. (7) and (8) along with the constitutive law [Eq. (1)]. We first turn the partial differential equation into a system of ordinary differential equations. We approximate the spatial derivatives using central second-order finite differences, with the diffusion term is split into two separate terms using the product rule. We write the spatial integral in Eq. (7) as a numerical integral using the trapezoidal method. Once the STZ equations are written as a system of ordinary differential equations, we use a second order linearly implicit trapezoidal method to advance the system in time. Because stick-slip events involve longer periods of elastic loading followed by rapid failure, we use an adaptive time stepping method to efficiently resolve the slider motion.

We vary the scaled driving rate from $V_0 = 10^{-12}$ to 10^{-4} , and vary the scaled spring stiffness at each velocity to find where the transition from steady sliding to stick-slip occurs. The other parameters are given in Table I. For each set of V_0 and k , we start the block at steady sliding. If the stress and slider velocity do not remain constant, then steady sliding is unstable. Figure 3(a) illustrates an example of the stress evolution when steady sliding is unstable—the shear stress begins to oscillate, and the oscillations grow into stick-slip cycles.

We compare slider motion in cases involving dynamic formation of a shear band with deformation that is homogeneous. To obtain homogeneous deformation, we start the system with a spatially homogeneous effective temperature. In contrast, to form a shear band, a small perturbation of the form $\delta\chi \operatorname{sech}(z/\delta z)$ is added to the initial effective temperature. We find that the values of $\delta\chi$ and δz do not influence the limit cycle of stick-slip motion nor the final width or amplitude of the shear band. For simplicity, we use values of

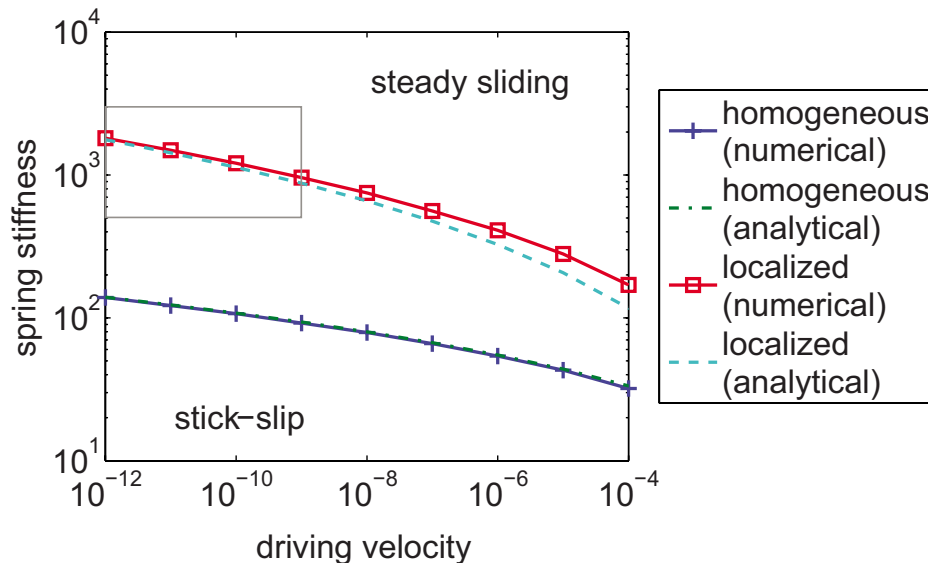


FIG. 4. (Color online) Comparison of analytical and numerical investigations of stick-slip. The plot shows the critical stiffness as a function of driving rate for the analytic expressions for homogeneous deformation and localized deformation [Eqs. (11) and (15), respectively] and the results obtained through numerical integration of the STZ equations. If the stiffness and driving rate are above the curve, then steady sliding is stable. If the values of the stiffness and driving rate are below the curve, motion occurs through stick-slip cycles. The analytical result for homogeneous shear matches extremely well with the numerical results. The prediction for localized deformation provides a good approximation of the shape of the boundary between stick-slip and steady sliding. The small discrepancy is due to the difficulty of estimating the shear band width a , as well as the fact that the strain rate is not constant in the shear band. The gray box indicates the region of parameter space where localized deformation produces multiple period stick-slips. This region is examined in detail in Fig. 5.

$\delta\chi=10^{-4}$ and $\delta z=0.1$ for all of our localized simulations.

Figure 4 shows the phase diagram in (V_0, k) space that result from our analytical and numerical studies. As expected, the critical stiffness decreases with the driving rate, and the critical stiffness for localized deformation is larger than that for homogeneous shear. The analytical expression for the critical stiffness with homogeneous shear matches extremely well with the numerical results. For localized deformation, our analysis yields a curve that is slightly below the curve obtained numerically. This discrepancy is due to the approximations we used to estimate the shear band width and the magnitude of the diffusion term. Changing the value of the correction factor in the prediction of the shear band thickness a [Eq. (14)] does not improve the analytical predictions. If the value of this factor is changed from 3.7 to 3 or 4.5, the prediction of the critical stiffness decreases by 10% in both cases. As mentioned above, the critical stiffness decreases as the correction factor is either increased or decreased due to the competing effects of dissipation and diffusion.

Our numerical results also indicate that the transition from steady sliding to stick-slip is continuous. As the stiffness is increased toward the critical stiffness, the amplitude of stick-slip cycles approaches zero. The transition is continuous at all velocities tested in our study.

We also use numerical integration to explore the dynamics of stick-slip. We do not observe complex stick-slip cycles for the homogeneous case. We find that localization produces irregular stick-slip cycles in certain regions of parameter space. Simultaneous observations of irregular stick-slip and the internal effective temperature dynamics establish a connection between the small scale physics and exotic macroscopic dynamics.

Multiple period stick-slip occurs for the lowest driving rates in our study, as shown in Fig. 5. This is a closer look at the gray box at the far left of Fig. 4, just below the localized transition from steady sliding to stick-slip. We see that there are many types of motion that occur in this small part of parameter space, including steady sliding, single period stick-slip, double period stick-slip, many (>2) period stick-slip, and material failure. Material failure refers to the fact that the strain rate becomes so large that the effective temperature diverges. Deformation in the amorphous material no longer occurs in isolated STZs at these large strain rates, and instead the deformation is more fluid-like. In the laboratory, stick-slip cycles are still likely to occur in this regime, but would require additional physics not included in STZ theory to be accurately captured theoretically.

We look at two specific examples of the irregular slider dynamics, one example that exhibits two period stick-slip (the “+” in Fig. 5), and one example that exhibits many irregular stick-slip cycles (the “x” in Fig. 5). Figure 6(a) shows shear stress as a function of load point displacement for stick-slip cycles with a doubled period. This stick-slip motion occurs for localized deformation with $V_0=10^{-10}$ and $k=1100$. The motion consists of a pair of alternating large and small events. The shear stress builds up to the same level during the “stick” phase of motion in both events, but the sticking time between slips alternates between two values. The slider slips much further during the big event, which relaxes the spring and drops the stress to a lower level, resulting in a longer sticking time following the large event compared to the sticking time after the small event. Figure 6(b) shows the slider velocity as a function of load point displacement. The large events result in a block velocity that

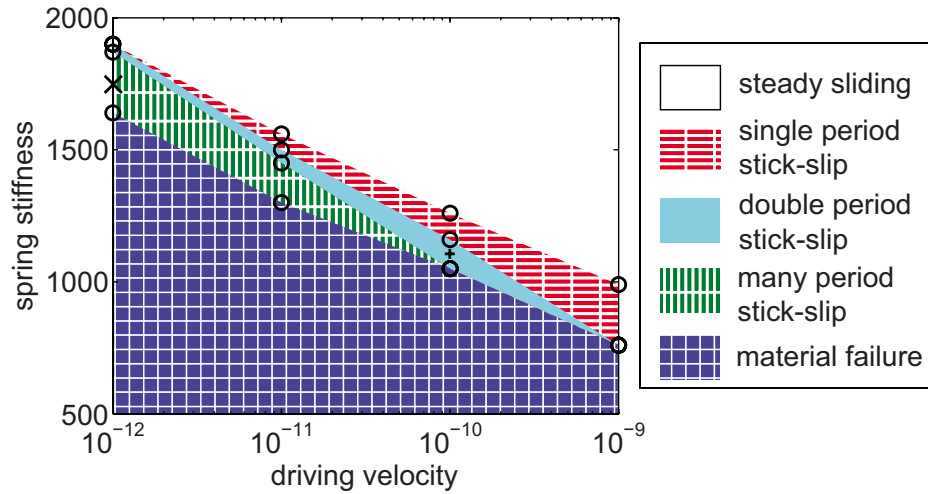


FIG. 5. (Color online) Diagram of parameter space where multiple period stick-slips do occur. This is a close up of the gray box at the far left of Fig. 4, just below the transition from steady sliding to stick-slip for localized deformation. In this smaller region of parameter space, many types of motion occur, including steady sliding, single period stick-slip, double period stick-slip, many (>2) period stick-slip, and material failure. All of the curves are plotted for localized deformation, as multiple period stick-slips does not occur for homogeneous shear. Material failure means that strain rates during the slip cycles are so large that STZ theory breaks down. A laboratory slider would likely still exhibits stick-slip motion in this part of parameter space, but additional physics would have to be added to STZ theory to model the motion theoretically. The circles indicate the specific values of k at fixed V_0 where we observe a transition from one type of stick-slip motion to another. The + at $V_0=10^{-10}$ indicates the specific example of double period stick-slip that we examine in Figs. 6 and 7, and the x at $V_0=10^{-12}$ indicates the specific example of many period stick-slip that we examine in Fig. 8.

is several orders of magnitude larger than in the small event. The slider moves slightly faster prior to the large event. However, the slider velocity is nearly an order of magnitude below the driving velocity during the “stick” phases prior to both events.

The slider slips more in the large event due to differences in the internal state of the material within the shear band—the strain rate profile in the material is different during large and small events. Both the slider velocity and the plastic strain rate are larger during the large stick-slip events. Small differences in the effective temperature have a large impact on the slider dynamics. Figure 7 (far left) shows shear stress as a function of load point displacement for a large and small stick-slip event which alternate in a two period cycle. At a series of four values of the shear stress, we plot the effective temperature as a function of z position within the layer. Because the shear stress is equal, differences in the stick-slip events must arise from differences in the internal dynamics of the effective temperature.

Figure 7(a) shows the effective temperature at the stress peaks. Prior to the large event, the effective temperature is slightly elevated at the center of the material. Dynamic feedbacks in the effective temperature evolution during slip amplify this difference. The slightly elevated effective temperature implies a higher density of STZs at the center of the material. The strain rate is also larger, and so the material dissipates more energy. Energy dissipation leads to faster growth of the effective temperature, which produces the profiles in Fig. 7(b). The differences is further amplified in Fig. 7(c), and in Fig. 7(d) the difference between the effective temperatures correspond to nearly a factor of 1000 increase in the plastic strain rate. As the effective temperature grows, the stress drops more rapidly during the large event due to

dynamic weakening. Because the stress drop is larger, the block slides farther due to the decreased frictional resistance.

This mechanism leads to further period doublings as the spring stiffness decreases, until the cycles are irregular. Figure 8(a) shows the shear stress as a function of load point displacement for a series of irregular stick-slip events. This block slider system is driven at $V_0=10^{-12}$ with a spring stiffness of $k=1700$. The shear stress at which the slip cycle begins is very similar for both smaller and larger events. Figure 8(b) shows the evolution of stress and slider velocity during the four stick-slip events in the gray box in Fig. 8(a). The slider velocity ranges over many orders of magnitude in the slip events. There is variation in the block velocity during the stick phase, though it is always well below the load point velocity V_0 , shown by the horizontal line. The block velocity during the stick phase is largest following a small event and smallest after a large event. However, the slider velocity during the stick phase is not completely indicative of the size of the next event, as the slider velocity during the stick phase takes on a range of values prior to both large and small slip events.

Figures 8(a) also shows that there are groups of smaller slip events followed by a larger slip event. The groups often have three or four stick-slip events, with several small events followed by a large event. Consecutive large events can also occur, as can be seen around a load point displacement of 0.3 in Fig. 8(a). The consecutive large events exhibit a smaller stress drop than the large events in the set of three or four events.

The small scale physics of strain localization leads to the various sizes of slip events due to the same mechanism described above for the double period stick-slip cycles. The effective temperature is largest in the center of the material

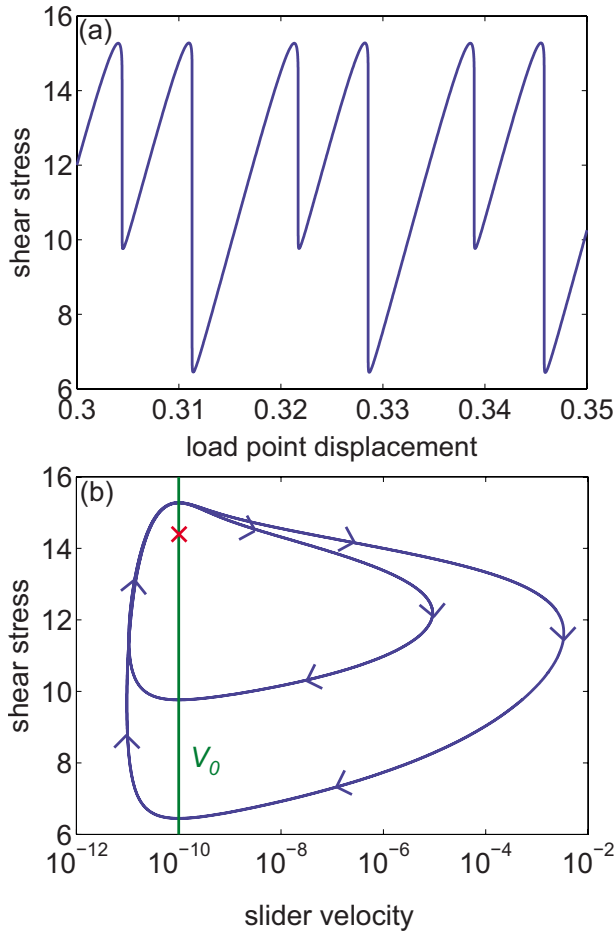


FIG. 6. (Color online) Two period stick-slip, with $V_0 = 10^{-10}$ and $k = 1100$. This point in the parameter space is shown by a + in Fig. 5. (a) Shear stress as a function of load point displacement. Instead of a single stick-slip event, there are two different stress drop sizes. The stress builds up to the same level to initiate failure in both event sizes, but the recurrence time differs between the events. The block slips more in the large event due to the microscopic effects of localization. (b) Stress and slider velocity evolution during two period stick-slips. The slider velocity is several orders of magnitude larger in the large stick-slip event. The velocity evolution during the stick phase leading up to failure is very similar in the large and small events. The stick-slip events have different sizes because of the internal effective temperature profile, which we examine in detail in Fig. 7.

prior to the largest events, and then dynamic feedbacks cause the effective temperature to grow more rapidly, similar to the plots in Fig. 7. The transitions to complex, chaotic behavior in our model arise from variations in the internal state of the material rather than instabilities associated with three (or more) macroscopic phenomenological degrees of freedom in a dynamic system, providing physical insight into the mechanisms that give rise to exotic friction behavior.

IV. DISCUSSION

Our study shows that strain localization plays an important role in stick-slip instabilities in amorphous materials.

The critical spring stiffness is larger for localized deformation than for homogeneous deformation and our analytic expressions for the critical stiffness are in good agreement with numerical integration. The primary effect that increases the critical stiffness for localized strain is an increase in the strain rate in the shear band. Diffusion also plays a role by mitigating the increase in the critical stiffness, though the increased strain rate is the dominant effect in determining the stability of steady sliding. Our analysis shows that the localization effect cannot be replicated in a homogeneous model by simply reducing the thickness of the material, and that resolving the microscopic dynamics is important for capturing the large scale friction.

Other constitutive laws such as Dieterich-Ruina also predict stick-slip motion [12]. In the Dieterich-Ruina law, the critical stiffness is independent of the driving rate, while in STZ theory the stiffness decreases with increasing driving rate. This general trend is in agreement with laboratory experiments [33], and previous studies with STZ theory that did not resolve the dynamic strain localization instability [15].

We also find that localized stick-slip can occur in irregular cycles. The effective temperature profile immediately before large and small events is slightly different, and this change in the microscopic physical state leads to macroscopically different friction dynamics. Phenomenological constitutive laws find that stick-slip can occur with irregular periods, though this requires additional state variables to provide the degrees of freedom necessary for chaotic stick-slip [13]. Our model instead relates irregular stick-slip to the internal physics of localization.

Many experiments show irregular stick-slip [1,8,34]. The exotic phenomena could arise from many different sources of complexity such as additional time scales associated with the apparatus and/or complex molecules in the interfacial layer which have their own internal dynamics or entanglements. Our study shows that even for simple interfacial materials, the small scale physics of strain localization can also be a source of complexity. Experiments on simpler amorphous materials that can simultaneously examine the dynamics of strain localization (e.g., experiments that can image particle displacements) could examine the region in parameter space where we observe irregular stick-slip to test the connection STZ theory makes between the microscopic physics and the microscopic dynamics.

Our model assumes that the effective temperature is only a function of position across the layer thickness. This simplifies the modeling, but experiments show that amorphous materials are heterogeneous in other spatial directions [35]. Extending slider models to additional dimensions may be important for fully capturing the complex stick-slip dynamics seen in various experiments.

Molecular dynamics simulations of amorphous materials show that stick-slip motion often occurs due to a phase transition from a solid to a fluid in the material [16]. This behavior is also observed in experiments [5]. The STZ model does not include the physics of this transition—melting occurs at the strain rate where the effective temperature diverges, but STZ theory does not include a constitutive description of the material once it melts. At these high strain rates, plastic de-

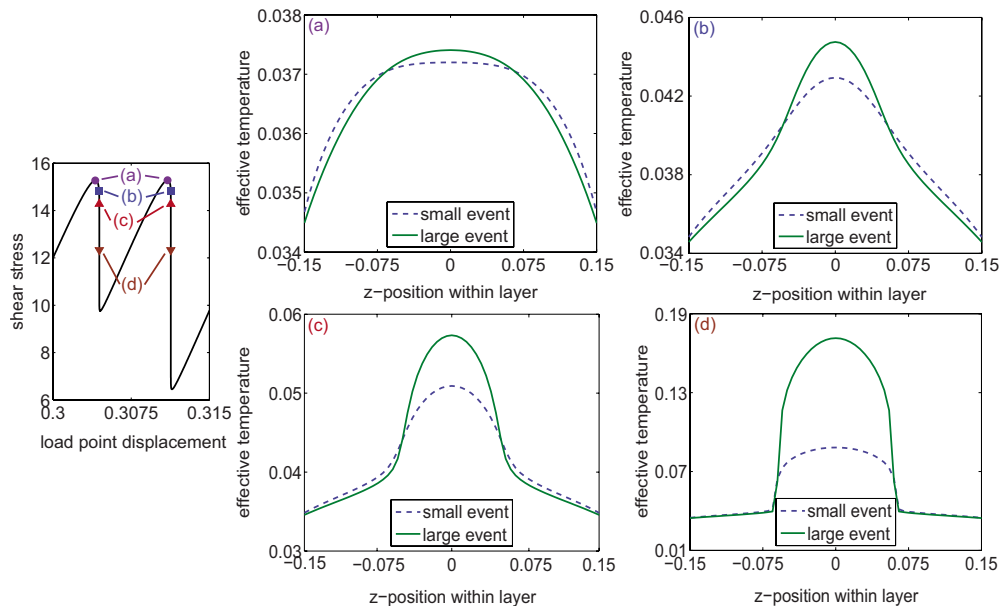


FIG. 7. (Color online) Close up of the effective temperature shear band in large and small stick-slip events. The far left plot shows the shear stress as a function of load point displacement for a large and a small stick-slip event. At four different values of the stress, shown by the dots on the two different curves, we plot the effective temperature profile across the layer (z direction). Because the stress is identical for the pair of curves in each of the four plots, the only difference between the block sliders is the effective temperature profile—the physical internal state of the sheared material is responsible for any differences in the dynamics. (a) At the peak stress prior to the slip event, the effective temperature profile is slightly different—the shear band is narrower and the effective temperature is larger in the center prior to the large event. (b) Because of feedbacks in the effective temperature dynamics, this difference is amplified, and the elevated effective temperature in the center point grows faster during the large event. This further increases the effective temperature at the center as the plots in (c) and (d) illustrate. Because the effective temperature is larger during the small event, the strain rate is larger and the shear stress drops to a lower value due to dynamic weakening. This is why the shear stress in the large event drops nearly twice as much as in the small event.

formation no longer occurs in isolated STZs, and the material instead flows like a fluid. Future modeling efforts that incorporate this melting transition can determine its effects on stick-slip for comparison with simulations and experiments.

Experiments could determine the thickness of shear bands during stick-slip motion to test our quantitative predictions for the effect of localization. In thin films, the material is often only a few molecules thick [34]. So, for these systems, localization may not be important as the shear band thickness may be wider than the entire material. In thicker materials such as granular materials, this effect is more likely to be important. Daniels and Hayman [1] observed stick-slip events in a granular material and imaged particle displacements before and after the event. They found that slip occurred only over a few particle diameters in the layer for some of the stick-slip events. Experiments on granular materials where grains can be imaged, or experiments with fault gouge that examine gouge microstructures following the experiment [4] can determine the shear band thickness. Such experiments could potentially test our predictions for the effect of shear bands on stick-slip instabilities.

Our model for stick-slip does not include inertial effects. We assume that the frictional time scale dominates stick-slip motion and that oscillations of the spring/mass system occur much faster than the inverse plastic strain rate time scale. Inertial effects are important in some regimes [17] and can be included in the block slider equations for numerical stud-

ies. However, these dynamical systems involve additional variables and analytical studies are consequently much more difficult. Stick-slip motion may require that the inverse plastic strain rate, mass/spring oscillation time, and stress equilibration time all be similar. This requires substantially more complicated modeling to resolve stress equilibration and wave propagation through the amorphous material. Addition of a mass resulted in chaotic motion with Dieterich-Ruina friction [36], so inertial dynamics could produce interesting dynamic phenomena in the STZ model.

Stick-slip instabilities are an important aspect of friction that must be understood to better constrain the dynamics of interfaces. Our results show that strain localization plays an important role in the macroscopic dynamics. Increasing the resolution of other relevant small scale phenomena in models of macroscopic dynamics should ultimately improve our ability to predict the deformation and failure in amorphous materials.

ACKNOWLEDGMENTS

This work was supported by the David and Lucile Packard Foundation, NSF Grant Number DMR-0606092 and the NSF/USGS Southern California Earthquake Center, funded by NSF Cooperative Agreement No. EAR-0106924 and USGS Cooperative Agreement No. 02HQAG0008. The SCEC contribution number for this paper is 1319.

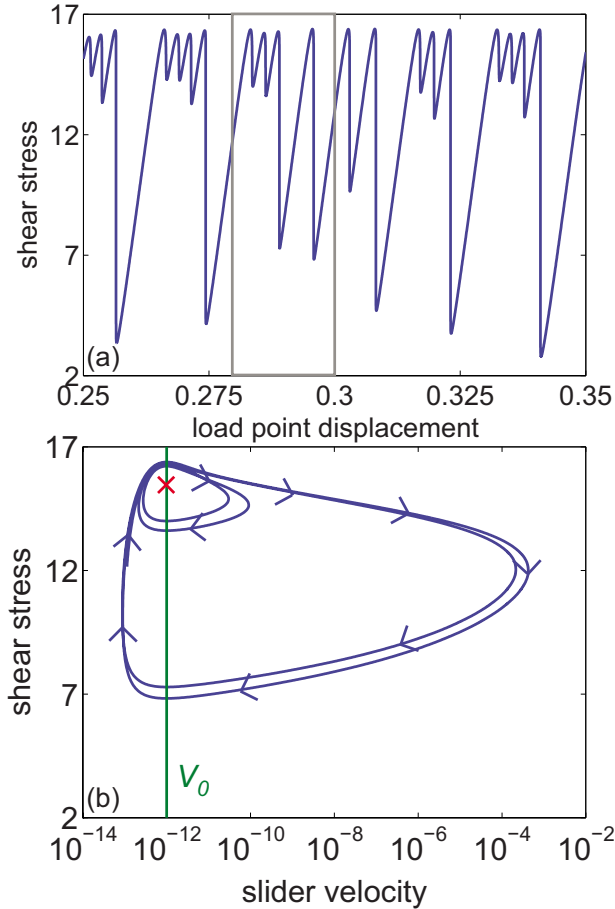


FIG. 8. (Color online) Irregular stick-slip events due to strain localization, with $V_0 = 10^{-12}$ and $k = 1700$. This point in parameter space is shown by an x in Fig. 4. (a) Shear stress as a function of load point displacement. Stress drops of many sizes occur, with irregular recurrence times. The peak stress is similar for all events, though there are some small variations. Events usually occur in groups of two or three small events followed by a large event, but there can also be several consecutive larger events. (b) Stress and slider velocity evolution during complex stick-slip cycles. The plot shows the four stick-slip cycles in the gray box in (a). The innermost loop is the first small stick-slip and the subsequent events are progressively larger. The vertical line indicates the load point velocity V_0 . The block velocity during sliding varies over many orders of magnitude. During the stick phase, there is variation in the velocity of the block. Small events are followed by increased block velocity during the stick phase, while the slider velocity is lower after large events. However, the slider velocity prior to a slip event does not determine its size.

APPENDIX A: FULL DERIVATION OF THE STZ EQUATIONS

STZ theory relates the plastic strain rate $\dot{\gamma}$ to the shear stress τ and the effective temperature χ [29]. The shear stress quantifies the rate at which STZs switch orientations and the effective temperature determines the total number of STZs in the material. Here, we present the details of the assumptions of the theory and derive the STZ equation used in this paper [Eq. (1)].

In STZ theory, plastic strain occurs in localized soft spots that are susceptible to rearrangement under applied shear

stress. These regions, called STZs, switch between two metastable orientations, denoted “positive” and “negative.” In the model, an STZ changing from positive to negative accumulates a positive fixed strain increment, and an STZ changing from negative to positive accumulates a negative fixed strain increment. An STZ undergoing a switch from positive to negative is shown in Fig. 1 (rightmost figure). An STZ in the negative orientation cannot shear further at that location, and to sustain plastic flow STZs are constantly created and destroyed as energy is dissipated in the material.

Quantitatively, the basic premise of STZ theory can be written as follows:

$$\dot{\gamma} = \frac{2\epsilon}{n_\infty t_0} [R(+\tau)n_+ - R(-\tau)n_-]. \quad (\text{A1})$$

The plastic strain rate $\dot{\gamma}$ is found from the number of STZs in each orientation, n_+ and n_- , and the rate at which STZs change orientation. The rate switching function $R(\tau)$ describes the rate at which STZ reversals take place in response to the applied shear stress. The other parameters are the strain increment per STZ reversal ϵ , a reference STZ population n_∞ , and the time scale for STZ reversals t_0 .

Equation (A1) is usually rewritten with the following change in variables:

$$\Lambda = \frac{n_+ + n_-}{n_\infty}, \quad m = \frac{n_- - n_+}{n_+ + n_-}. \quad (\text{A2})$$

The variable Λ is proportional to the total number of STZs and m quantifies the bias. After performing this change in variables, Eq. (A1) becomes

$$\dot{\gamma} = \frac{2\epsilon}{t_0} \mathcal{C}(\tau) \Lambda [\mathcal{T}(\tau) - m]. \quad (\text{A3})$$

The constitutive law is written here with two functions of the rate switching function $\mathcal{C}(\tau) = [R(\tau) + R(-\tau)]/2$ and $\mathcal{T}(\tau) = [R(\tau) - R(-\tau)]/[R(\tau) + R(-\tau)]$.

We assume an exponential form for $R(\tau)$ [37]

$$R(\tau) = \exp(-f_0 + \tau/\sigma_d). \quad (\text{A4})$$

The rate switching function depends on an activation stress σ_d and an activation energy scaled by the energy required to form an STZ. This form for $R(\tau)$ is used in other formulations of STZ theory [15,38] and reproduces the logarithmic rate dependence of the Dieterich-Ruina law [21]. The rate switching function combinations are then $\mathcal{C}(\tau) = \exp(-f_0) \cosh(\tau/\sigma_d)$ and $\mathcal{T}(\tau) = \tanh(\tau/\sigma_d)$. For the parameters in our study, $\tau \gg \sigma_d$. Under this approximation, we set $\mathcal{T}(\tau) \approx 1$.

The STZ populations dynamically evolve as STZs switch between orientations and energy dissipation creates and destroys STZs. The evolution equations that we adopt for the STZ populations are

$$\frac{dn_{\pm}}{dt} = \frac{1}{t_0} [R(\mp \tau)n_{\mp} - R(\pm \tau)n_{\pm}] + \frac{\dot{\gamma}\tau}{\epsilon(n_{+} + n_{-})\tau_y} \left[\frac{n_{\infty}}{2} \exp(-1/\chi) - n_{\pm} \right]. \quad (\text{A5})$$

The first term accounts for STZs switching between the two possible orientations and the second term incorporates STZ creation and annihilation. The overall creation/annihilation rate is proportional to the rate at which energy is dissipated in the material. Energy dissipation in the material drives the STZ population toward a Boltzmann distribution, and the stress τ_y determines the fraction of dissipated energy that creates STZs. The stress τ_y also turns out to be the yield stress, the stress below which the material is jammed.

In the Λ and m variables, the evolution equations are

$$\frac{d\Lambda}{dt} = \frac{\dot{\gamma}\tau}{n_{\infty}\Lambda\tau_y} [\exp(-1/\chi) - \Lambda], \quad (\text{A6})$$

$$\frac{dm}{dt} = \frac{\dot{\gamma}}{\epsilon n_{\infty}\Lambda} \left\{ 1 - \frac{\pi m}{\tau_y} [1 + \exp(-1/\chi) - \Lambda] \right\}. \quad (\text{A7})$$

Note that both the Λ and m equations are inversely proportional to the number of STZs $n_{\infty}\Lambda$. STZ theory postulates that STZs occur in local, isolated regions. Therefore, because the number of STZs is small, the factor $1/(n_{\infty}\Lambda)$ is large, and the STZ populations evolve much faster than the stress and effective temperature. With this in mind, we assume the total number of STZs is always at its steady-state value $\Lambda = \exp(-1/\chi)$, which is set by the local effective temperature.

If we set the total number of STZs to steady state, then the STZ bias is $m = \tau_y/\tau$. The STZ bias cannot exceed $m=1$, which corresponds to all the STZs in the negative orientation. When this occurs, the material is jammed ($\dot{\gamma}=0$) and cannot be sheared further because there are no regions susceptible to deformation. If $\tau > \tau_y$, then the material flows. Therefore, the steady-state value for the STZ bias is dependent on the shear stress as follows:

$$m = \begin{cases} 1, & \tau < \tau_y \\ \tau_y/\tau, & \tau \geq \tau_y. \end{cases} \quad (\text{A8})$$

The STZ dynamics determine if the material is jammed or flowing, but otherwise the stress and effective temperature have the dominant effect on the friction dynamics.

If we set the STZ populations to their steady-state values, then we have the exact form for Eq. (1),

$$\dot{\gamma} = \frac{2\epsilon}{t_0} \exp(-f_0) \cosh[\pi/\sigma_d] \exp(-1/\chi) \left[1 - \frac{\tau_y}{\tau} \right], \quad (\text{A9})$$

unless $\tau < \tau_y$, in which case $\dot{\gamma}=0$. The strain rate depends on the shear stress and the internal physics of the material is described by the effective temperature. We discuss the dynamic equation for the effective temperature in Sec. II A in the main text.

APPENDIX B: LINEAR STABILITY ANALYSIS FOR THE STZ EQUATIONS

1. Homogeneous deformation

First, we perform the stability analysis with the assumption that the effective temperature is spatially homogeneous. In this case, the diffusion term in the effective temperature equation is zero and the spatial integral in Eq. (7) is $\int \exp(-1/\chi) dz = \exp(-1/\chi)$. The dynamical system for homogeneous deformation is

$$\dot{\tau} = k[V_0 - f(\tau)\exp(-1/\chi)], \quad (\text{B1})$$

$$\dot{\chi} = \frac{f(\tau)\exp(-1/\chi)\tau}{c_0} \left[1 - \frac{\chi}{\hat{\chi}(\dot{\gamma})} \right]. \quad (\text{B2})$$

The Jacobian of the STZ equations for homogeneous deformation is

$$J_{11} = \frac{\partial \dot{\tau}}{\partial \tau} = -kf'(\tau)\exp(-1/\chi), \quad (\text{B3})$$

$$J_{12} = \frac{\partial \dot{\tau}}{\partial \chi} = -\frac{kf(\tau)\exp(-1/\chi)}{\chi^2}, \quad (\text{B4})$$

$$J_{21} = \frac{\partial \dot{\chi}}{\partial \tau} = \frac{[f'(\tau)\tau + f(\tau)]\exp(-1/\chi)}{c_0} \left(1 - \frac{\chi}{\hat{\chi}} \right) + \frac{f(\tau)\exp(-1/\chi)\tau}{c_0} \frac{\chi}{\hat{\chi}^2} \frac{\partial \hat{\chi}}{\partial \tau}, \quad (\text{B5})$$

$$J_{22} = \frac{\partial \dot{\chi}}{\partial \chi} = \frac{f(\tau)\exp(-1/\chi)\tau}{c_0\chi^2} \left(1 - \frac{\chi}{\hat{\chi}} \right) + \frac{f(\tau)\exp(-1/\chi)\tau}{c_0} \left(\frac{\chi}{\hat{\chi}^2} \frac{\partial \hat{\chi}}{\partial \chi} - \frac{1}{\hat{\chi}} \right). \quad (\text{B6})$$

The maximum effective temperature is a function of the strain rate, which means that $\hat{\chi}$ depends on both the stress and the effective temperature. When evaluated at steady state [$V_0 = f(\tau)\exp(-1/\chi)$ and $\chi = \hat{\chi}$], this becomes

$$J_{11} = \frac{\partial \dot{\tau}}{\partial \tau} = -\frac{kf'(\tau)V_0}{f(\tau)}, \quad (\text{B7})$$

$$J_{12} = \frac{\partial \dot{\tau}}{\partial \chi} = -\frac{kV_0}{\chi^2}, \quad (\text{B8})$$

$$J_{21} = \frac{\partial \dot{\chi}}{\partial \tau} = \frac{V_0\tau\hat{\chi}f'(\tau)}{c_0\chi_w f(\tau)}, \quad (\text{B9})$$

$$J_{22} = \frac{\partial \dot{\chi}}{\partial \chi} = \frac{V_0\tau}{c_0\hat{\chi}} \left(\frac{1}{\chi_w} - 1 \right), \quad (\text{B10})$$

since the derivatives of $\hat{\chi}$ with respect to stress and effective temperature are

$$\frac{\partial \hat{\chi}}{\partial \tau} = \frac{\hat{\chi}^2 f'(\tau)}{\chi_w f(\tau)}, \quad (\text{B11})$$

$$\frac{\partial \hat{\chi}}{\partial \chi} = \frac{\hat{\chi}^2}{\chi^2} \frac{1}{\chi_w}. \quad (\text{B12})$$

The real part of the eigenvalues is the trace of the Jacobian, as near the transition from stable sliding to unstable sliding, the eigenvalues are complex. Steady sliding is unstable if the trace of the Jacobian is greater than zero,

$$\text{Tr}(J) = \frac{\partial \dot{\tau}}{\partial \tau} + \frac{\partial \dot{\chi}}{\partial \chi} = -\frac{kV_0 f'(\tau)}{f(\tau)} + \frac{V_0 \tau}{c_0 \hat{\chi}} \left(\frac{1}{\chi_w} - 1 \right) > 0. \quad (\text{B13})$$

Equation (9) reveals that stability is determined by two competing effects. The first term in Eq. (B13) comes from the spring force. This term is always negative, as the spring force is always a restoring force that pushes the block toward equilibrium. The second term in Eq. (9) comes from the energy dissipation term in the effective temperature evolution equation. This term is destabilizing only if $\chi_w < 1$ (i.e., for rate weakening parameters).

2. Localized deformation

We now determine the role of localization by performing a linear stability analysis on the full STZ equations [Eqs. (7) and (8)]. This involves the same steps as the homogeneous case, but with the inclusion of the diffusion term in Eq. (8) and the spatial integral in Eq. (7). We study how perturbations to a steady shear band solution to the effective temperature equations grow in time. To simplify the analysis, we assume that the perturbations to the effective temperature are not a function of z . Spatially varying perturbations can be considered through an analysis of normal modes. However, it turns out that the zero wavenumber mode is the least stable [the diffusion term in Eq. (8) results in the higher wavenumber modes being more stable], so nothing extra is gained with a perturbation that varies with z .

For localized deformation, the Jacobian of the system is

$$J_{11} = \frac{\partial \dot{\tau}}{\partial \tau} = -kf'(\tau) \int_0^1 \exp(-1/\chi) dz, \quad (\text{B14})$$

$$J_{12} = \frac{\partial \dot{\tau}}{\partial \chi} = -kf(\tau) \int_0^1 \frac{\exp(-1/\chi)}{\chi^2} dz, \quad (\text{B15})$$

$$J_{21} = \frac{\partial \dot{\chi}}{\partial \tau} = \frac{[f'(\tau)\tau + f(\tau)] \exp(-1/\chi)}{c_0} \left(1 - \frac{\chi}{\hat{\chi}} \right) + \frac{f(\tau) \exp(-1/\chi) \tau}{c_0} \frac{\partial \hat{\chi}}{\hat{\chi}^2 \partial \tau} + Df'(\tau) \frac{\partial}{\partial z} \left[\exp(-1/\chi) \frac{\partial \chi}{\partial z} \right], \quad (\text{B16})$$

$$J_{22} = \frac{\partial \dot{\chi}}{\partial \chi} = \frac{f(\tau) \exp(-1/\chi) \tau}{c_0 \chi^2} \left(1 - \frac{\chi}{\hat{\chi}} \right) + \frac{f(\tau) \exp(-1/\chi) \tau}{c_0} \left(\frac{\chi}{\hat{\chi}^2} \frac{\partial \hat{\chi}}{\partial \chi} - \frac{1}{\hat{\chi}} \right) + Df(\tau) \frac{\partial}{\partial \chi} \left\{ \frac{\partial}{\partial z} \left[\exp(-1/\chi) \frac{\partial \chi}{\partial z} \right] \right\}. \quad (\text{B17})$$

Perturbations to the effective temperature are independent of z , so the χ derivative in the diffusion term in J_{22} only acts on the $\exp(-1/\chi)$ factor,

$$\frac{\partial}{\partial \chi} \left\{ \frac{\partial}{\partial z} \left[\exp(-1/\chi) \frac{\partial \chi}{\partial z} \right] \right\}, \quad (\text{B18})$$

$$= \frac{\partial}{\partial z} \left[\frac{\exp(-1/\chi)}{\chi^2} \frac{\partial \chi}{\partial z} \right], \quad (\text{B19})$$

$$= \frac{1}{\chi^2} \frac{\partial}{\partial z} \left[\exp(-1/\chi) \frac{\partial \chi}{\partial z} \right] - \frac{2 \exp(-1/\chi)}{\chi^3} \left(\frac{\partial \chi}{\partial z} \right)^2. \quad (\text{B20})$$

When evaluated at steady state, where $V_0 = f(\tau) \int \exp(-1/\chi) dz$ and the diffusion and energy dissipation terms balance, the Jacobian becomes:

$$J_{11} = \frac{\partial \dot{\tau}}{\partial \tau} = -\frac{kf'(\tau)V_0}{f(\tau)}, \quad (\text{B21})$$

$$J_{12} = \frac{\partial \dot{\tau}}{\partial \chi} = -kf(\tau) \int_0^1 \frac{\exp(-1/\chi)}{\chi^2} dz, \quad (\text{B22})$$

$$J_{21} = \frac{\partial \dot{\chi}}{\partial \tau} = \frac{f(\tau) \exp(-1/\chi)}{c_0} \left(1 - \frac{\chi}{\hat{\chi}} \right) + \frac{f(\tau) \exp(-1/\chi) \tau \hat{\chi} f'(\tau)}{c_0 \chi_w f(\tau)}, \quad (\text{B23})$$

$$J_{22} = \frac{\partial \dot{\chi}}{\partial \chi} = \frac{f(\tau) \exp(-1/\chi) \tau}{c_0 \hat{\chi}} \left(\frac{1}{\chi_w} - 1 \right) - \frac{2Df(\tau) \exp(-1/\chi)}{\chi^3} \left(\frac{\partial \chi}{\partial z} \right)^2. \quad (\text{B24})$$

As with homogeneous deformation, the eigenvalues turn out to be complex at steady state. The real part of the eigenvalues is the trace of the Jacobian. Therefore, if the trace of the Jacobian is greater than zero, steady sliding is unstable:

$$\text{Tr}(J) = \frac{\partial \dot{\tau}}{\partial \tau} + \frac{\partial \dot{\chi}}{\partial \chi} = -\frac{kV_0 f'(\tau)}{f(\tau)} + \frac{\gamma \tau}{c_0 \hat{\chi}} \left(\frac{1}{\chi_w} - 1 \right) - 2D \frac{\dot{\gamma}}{\chi^3} \left(\frac{\partial \chi}{\partial z} \right)^2 > 0. \quad (\text{B25})$$

There are two important differences between this expression and the equivalent expression for homogeneous deformation [Eq. (B13)]. First is the presence of the diffusion term, which is negative and therefore stabilizes the growth of perturba-

tions. The other important difference is that the energy dissipation term [the second term in Eq. (B25)] depends on the strain rate rather than the average strain rate. This term is much larger when a shear band forms due to the elevated

strain rate in the shear band. Ultimately this implies that stick-slip motion occurs for a larger spring stiffness when a shear band forms.

-
- [1] K. E. Daniels and N. W. Hayman, *J. Geophys. Res.* **113**, B11411 (2008).
- [2] W. F. Brace and J. D. Byerlee, *Science* **153**, 990 (1966).
- [3] W. F. Brace, *Tectonophysics* **14**, 189 (1972).
- [4] J. L. Anthony and C. J. Marone, *J. Geophys. Res.* **110**, B08409 (2005).
- [5] H. Yoshizawa and J. N. Israelachvili, *J. Phys. Chem.* **97**, 11300 (1993).
- [6] C. Drummond and J. Israelachvili, *Phys. Rev. E* **63**, 041506 (2001).
- [7] D. Gourdon and J. N. Israelachvili, *Phys. Rev. E* **68**, 021602 (2003).
- [8] H. Zeng, M. Tirrell, and J. Israelachvili, *J. Adhes.* **82**, 933 (2006).
- [9] P. J. Blau, *Friction and Wear Transitions of Materials: Break-in, Run-in, Wear-* (Noyes, Park Ridge, NJ, 1989), pp. 312–317.
- [10] J. H. Dieterich, *J. Geophys. Res.* **84**, 2161 (1979).
- [11] A. L. Ruina, Ph. D. thesis, Brown University, Providence, RI, 1980.
- [12] J. R. Rice and A. L. Ruina, *ASME J. Appl. Mech.* **50**, 343 (1983).
- [13] J. C. Gu, J. R. Rice, A. L. Ruina, and S. T. Tse, *J. Mech. Phys. Solids* **32**, 167 (1984).
- [14] A. A. Batista and J. M. Carlson, *Phys. Rev. E* **57**, 4986 (1998).
- [15] A. Lemaître and J. M. Carlson, *Phys. Rev. E* **69**, 061611 (2004).
- [16] P. A. Thompson and M. O. Robbins, *Science* **250**, 792 (1990).
- [17] B. Luan and M. O. Robbins, *Phys. Rev. Lett.* **93**, 036105 (2004).
- [18] M. L. Falk and J. S. Langer, *Phys. Rev. E* **57**, 7192 (1998).
- [19] M. L. Falk and J. S. Langer, *MRS Bull.* **25**, 40 (2000).
- [20] J. S. Langer and M. L. Manning, *Phys. Rev. E* **76**, 056107 (2007).
- [21] E. G. Daub and J. M. Carlson, *J. Geophys. Res.* **113**, B12309 (2008).
- [22] M. L. Manning, J. S. Langer, and J. M. Carlson, *Phys. Rev. E* **76**, 056106 (2007).
- [23] E. G. Daub, M. L. Manning, and J. M. Carlson, *Geophys. Res. Lett.* **35**, L12310 (2008).
- [24] M. L. Manning, E. G. Daub, J. S. Langer, and J. M. Carlson, *Phys. Rev. E* **79**, 016110 (2009).
- [25] J. Lu, G. Ravichandran, and W. L. Johnson, *Acta Mater.* **51**, 3429 (2003).
- [26] J.-C. Tsai and J. P. Gollub, *Phys. Rev. E* **72**, 051304 (2005).
- [27] J. Lauridsen, M. Twardos, and M. Dennin, *Phys. Rev. Lett.* **89**, 098303 (2002).
- [28] G. Lois, A. Lemaitre, and J. M. Carlson, *Phys. Rev. E* **72**, 051303 (2005).
- [29] J. S. Langer, *Phys. Rev. E* **77**, 021502 (2008).
- [30] Y. Shi, M. B. Katz, H. Li, and M. L. Falk, *Phys. Rev. Lett.* **98**, 185505 (2007).
- [31] T. K. Haxton and A. J. Liu, *Phys. Rev. Lett.* **99**, 195701 (2007).
- [32] J. M. Carlson and A. A. Batista, *Phys. Rev. E* **53**, 4153 (1996).
- [33] T. Baumberger, F. Heslot, and B. Perrin, *Nature (London)* **367**, 544 (1994).
- [34] C. Drummond and J. Israelachvili, *Macromolecules* **33**, 4910 (2000).
- [35] T. S. Majmudar and R. P. Behringer, *Nature (London)* **435**, 1079 (2005).
- [36] B. Erickson, B. Birnir, and D. Lavalée, *Nonlinear Processes Geophys.* **15**, 1 (2008).
- [37] H. J. Eyring, *J. Chem. Phys.* **4**, 283 (1936).
- [38] A. Lemaître, *Phys. Rev. Lett.* **89**, 195503 (2002).